

太陽光エネルギーの有効利用を目指した金属クラスター型人工光合成モデルの構築
**Artificial photosynthetic model composed of noble metal clusters towards efficient
utilization of sunlight**

研究代表者 北海道大学 大学院工学研究院 助教 石田 洋平

Yohei Ishida, Assistant Professor of Faculty of Engineering, Hokkaido University

1. Abstract

I have been studying the control of molecular assembly structure based on electrostatic interaction and its application to artificial photosynthetic systems. Recently, I have succeeded in synthesizing a group of cationic metal clusters with a completely single composition for the first time. By applying the ordered assembly control technique to molecular metal clusters, I aimed to propose an artificial photosynthetic model. I synthesized new metal cluster compounds with surface charges, but it was difficult to isolate clusters with visible light emission due to the low thermal stability of the cluster compounds with very dense surface charges. I therefore tried to establish a new method to obtain cluster compounds with the desired composition while controlling the number of surface charges. Surface chemical reactions on atomically precise metal clusters have considerable attention for opening a new platform for cluster functionalization. In this study, basic $\text{Au}_{25}(\text{4-PyET})_{18}$ ($\text{4-PyET} = -\text{SCH}_2\text{CH}_2\text{Py}$; $\text{Py} = \text{pyridyl}$) clusters were successfully transformed into cationized $\text{Au}_{25}(\text{4-PyET}\cdot\text{CH}_3^+)_{x}(\text{4-PyET})_{18-x}$ clusters, without altering their Au_{25} cores, through the Menshutkin $\text{S}_{\text{N}}2$ reaction of their surface Py moieties. This study offers not only a simple cationization method, but also a protocol for modifying the surface functionalities of molecular metal clusters via a synthetic reaction. The use of metal clusters as supramolecular devices with functional sites on the surface is now in progress.

2. Introduction

Photosynthesis in natural plants is one of the ideal photochemical reactions. It is an extremely efficient light-harvesting system that collects visible light and realizes light energy conversion reactions using water as an electron source. In the light-harvesting system, the chlorophyll pigments are appropriately aligned and oriented by the surrounding proteins, resulting in highly efficient light energy collection and transfer. Based on the guideline that regular molecular arrangements are important for highly efficient photochemical reaction systems, research is being conducted worldwide. Although covalent linkage is a typical method for constructing a regular assembly

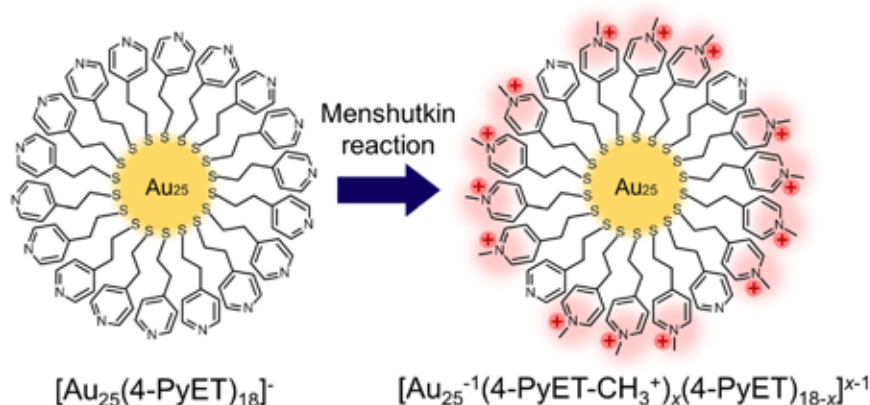
structure of organic molecules, I have succeeded in precisely controlling the assembly structure of molecules based on electrostatic interactions for anionic inorganic nanosheet materials, and have constructed an artificial light-harvesting model with almost 100% quantum efficiency and a new artificial photosynthesis model.

In this study, we focused on the possibility of using atomically precise molecular metal cluster compounds as a chemical reaction field in order to mimic the precise molecular arrangement structure of the photosynthetic system in a three-dimensional system. Atomically precise, thiolate-protected gold clusters ($\text{Au}_m(\text{SR})_n$) have potential applications in diverse fields, such as catalysis,^{1,2} sensing,^{3,4} and bio-applications,^{5,6} owing to their interesting physicochemical properties. Surface SR ligands are of particular interest as they affect the magic size (stable number of metal atoms) and structures of the clusters.^{6,7} Furthermore, the R-groups on the cluster surface are exposed to solutions and other phases; hence, they determine the molecular-like characteristics of clusters,⁸ such as their hydrophobicities/hydrophilicities,⁹ chiralities,¹⁰ catalytic activities,^{2,11} optical properties,¹² and interactions with host materials.^{5,6} These R-groups are therefore crucial to the rational design of the functional properties and applications of clusters. In peculiar, clusters capped by cationic R-groups are desirable as they widen the applications of bioimaging and sensing;¹³ however, the synthesis of cationized clusters is rarely reported owing to the difficulty in handling the positive charges of R-groups.¹⁴⁻¹⁶ By preventing the formation of $[\text{Au}(\text{I})-\text{SR}^+]$ ionic polymer complexes that hinder the homogeneous reduction of Au precursors and the formation of atomically pure clusters, we recently succeeded in the synthesis of cationized Au clusters ($\text{Au}_{25}(\text{S}(\text{CH}_2)_{11}\text{N}(\text{CH}_3)_3^+)_{18}$,¹⁴ $\text{Au}_{144}(\text{S}(\text{CH}_2)_{11}\text{N}(\text{CH}_3)_3^+)_{60}$,¹⁵ and $\text{Au}_{25}(\text{S}(\text{CH}_2)_{11}\text{N}(\text{CH}_3)_3^+)_x(\text{S}(\text{CH}_2)_2\text{Ph})_{18-x}$ ($x=1-6$)).¹⁶

To date, major protocols for the preparation of atomically precise clusters with various thiolate ligands have been categorized into size-focusing^{14,15} and ligand-exchange method.^{16,17} In the former case, the $\text{Au}(\text{I})-\text{SR}$ complex is prepared by mixing Au ion and thiols (HSR), followed by reduction into objected Au clusters. The latter involves the synthesis of Au clusters, followed by the replacement of their initial ligands with the desired ligands. Besides these methods, surface reactions have also received significant attention in recent years; however, there are few reports on such reactions, two of which are azido- and amide-bond formation reactions.^{18,19}

The Menshutkin $\text{S}_{\text{N}}2$ reaction is a common method to obtain quaternary ammonium salt ($[\text{-N}(\text{CH}_3)_3]^+$) by reacting a tertiary amine with an alkylating agent.²⁰ In this study, we demonstrate the Menshutkin (methylation) reaction of the surface pyridyl (Py) moieties on basic $\text{Au}_{25}(4\text{-PyET})_{18}$ clusters ($4\text{-PyET} = \text{-SCH}_2\text{CH}_2\text{Py}$) for their successful

transformation into cationized $\text{Au}_{25}(\text{4-PyET-CH}_3^+)_x(\text{4-PyET})_{18-x}$ ($x \approx 18$) clusters (Scheme 1). This work proposes a novel strategy for not only the cationization of Au clusters by surface chemical reactions, but their functionalization as well.



Scheme 1 Menshutkin (methylation) reaction on $\text{Au}_{25}(\text{4-PyET})_{18}$ clusters
 (4-PyET = $-\text{SCH}_2\text{CH}_2\text{Py}$, where Py = pyridyl group)

3. Results and Discussion

The following 4 chemicals were evaluated as methylating reagents: iodomethane (MeI), dimethyl sulfate (Me_2SO_4), methyl trifluoromethanesulfonate (TfOMe), and trimethyl oxonium tetrafluoroborate (Me_3OBF_4) (reactivity with Py group: $\text{MeI} < \text{Me}_2\text{SO}_4 < \text{TfOMe} < \text{Me}_3\text{OBF}_4$). The surface-reactive basic Au cluster $\text{Au}_{25}(\text{4-PyET})_{18}$ was synthesized according to our method as reported previously and characterized by electrospray ionization mass spectrometry (ESI-MS) and UV-vis absorption.²¹ Figures 1(a)-(d) show the UV-vis absorption spectra of the samples before (0 min) and after the methylation reaction (30 min or 60 min) using each of the 4 methylating reagents. When MeI and Me_3OBF_4 were used (Figures 1(a) and (d), respectively), the characteristic absorption peaks of Au_{25} clusters^{22,23} at 400, 450, 560, 670 and 780 nm disappeared after the reaction, indicating that these reagents decomposed the Au_{25} clusters. On the other hand, no obvious decreases in the absorption spectra were observed when using Me_2SO_4 and TfOMe (Figures 1(b) and (c)). The decomposition of the clusters by MeI is due to the nucleophilicity of the I⁻ ion generated by the reaction, as reported elsewhere.²⁴ Besides, methylating agents not only react with the Py group of the ligands, but with the $-\text{S}$ moiety of the Au-S bonds as well. Their reaction with the $-\text{S}$ group causes the Au-S bond to break, leading to the decomposition of the clusters. Me_3OBF_4 likely decomposed the clusters owing to its strong reactivity. On the other hand, Me_2SO_4 and TfOMe

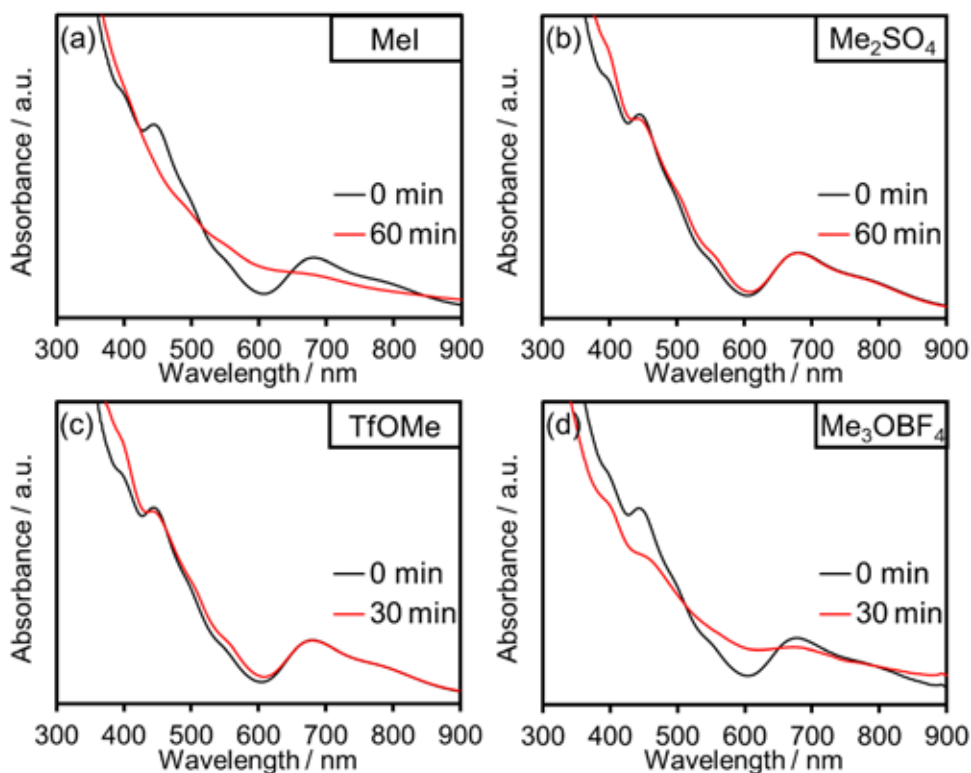


Figure 1 Selection of methylating reagents

(UV-vis absorption spectra of the samples before (0 min) and after reaction (30 min or 60 min) with (a) MeI, (b) Me₂SO₄, (c) TfOMe, and (d) Me₃OBF₄)

selectively react with the outer Py groups over the inner –S groups because of their moderate reactivity, allowing the methylation reaction to proceed without any decomposition of the clusters.

TfOMe, which proceeded the most efficiently, was selected as the methylating reagent. The Menshutkin reaction on the Au₂₅(4-PyET)₁₈ cluster was conducted to obtain methylated, cationized Au₂₅ clusters (see the detailed procedure in the Supporting Information). Trifluoromethanesulfonic acid (CF₃SO₂OH) was noted as a decomposition product of TfOMe, which could hinder the Menshutkin reaction by protonating the unreacted Py groups. By performing the 1h reaction 3 times (i.e., 3 cycles), CF₃SO₂OH was effectively removed and the reaction was proceeded efficiently. Notably, running 1 cycle for up to 2 days did not produce fully methylated Au clusters as the main product and was less efficient than the 3-cycle reaction. UV-vis absorption spectra of the sample before and after 1 cycle showed slight increases in the characteristic Au₂₅ cluster bands^{22,23} at 400 and 560 nm, whereas those at 450, 670, and 780 nm slightly decreased (Figure 2). Such absorption changes were also observed when Au₂₅(4-PyET)₁₈ clusters

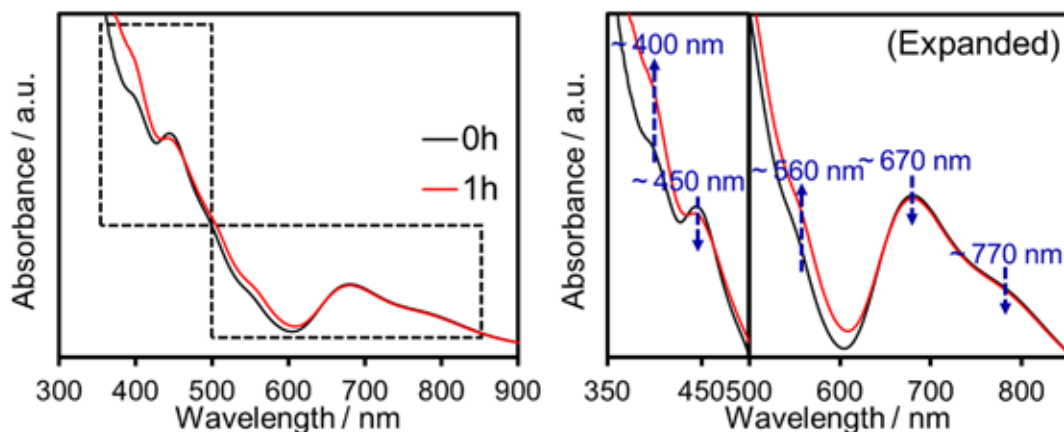


Figure 2 UV-vis absorption spectra of the sample before (0h) and after 1-cycle reaction (1h) with TfOMe

were treated with HCl, in which the reversible protonation of the Py group gave its positive form, $-C_5H_4NH^+$.²¹ These results strongly suggest that the geometric structure of Au₂₅ core was distorted due to the surface charge anisotropy^{12,21} during the addition of positive charges. The absorption spectra showed negligible changes after the 2nd and 3rd reaction cycles, demonstrating the good stability of the methylated, cationized Au₂₅ clusters and lack of geometrical changes in the Au₂₅ core (discussed in detail in Figure 4).

The positive-mode ESI-MS of the methylated Au₂₅ clusters (Figure 3, left) showed 3 different charged states +2, +3, and +4 (depending on the number of attached PF₆⁻ anions). Specifically, $[Au_{25}^{-1}(4-PyET-CH_3^+)_x(4-PyET)_{18-x} \cdot (PF_6^-)_{x-3}]^{2+}$ ($11 \leq x \leq 18$), $[Au_{25}^{-1}(4-PyET-CH_3^+)_x(4-PyET)_{18-x} \cdot (PF_6^-)_{x-4}]^{3+}$ ($12 \leq x \leq 18$), and $[Au_{25}^{-1}(4-PyET-CH_3^+)_x(4-PyET)_{18-x} \cdot (PF_6^-)_{x-5}]^{4+}$ ($14 \leq x \leq 18$) (groups Au₂₅(+2), Au₂₅(+3), and Au₂₅(+4), respectively) were observed. Figure 3 (right) shows the expanded ESI-MS of the methylated Au₂₅ clusters with +3 charged state (group Au₂₅(+3)) observed with relatively high intensity. After 1st reaction cycle (1h in total), the x values (the number of methylated ligands) ranged between 12 and 18. Note that after 2 min of reaction, x had already reached 10-18, indicating the reaction rate became very inefficient due to the decrease in the number of reaction sites and bulkiness of the counter anions CF₃SO₃⁻ and PF₆⁻, which geometrically impede further reaction of the unreacted ligands. After the 2nd and 3rd reaction cycles (2h and 3h in total, respectively), the x values increased to $x=14-18$ and $15-18$ respectively. The average number of methylated ligands was calculated from the peak intensity ratio, assuming the mass spectral signal intensities are equal to the solution concentrations of the

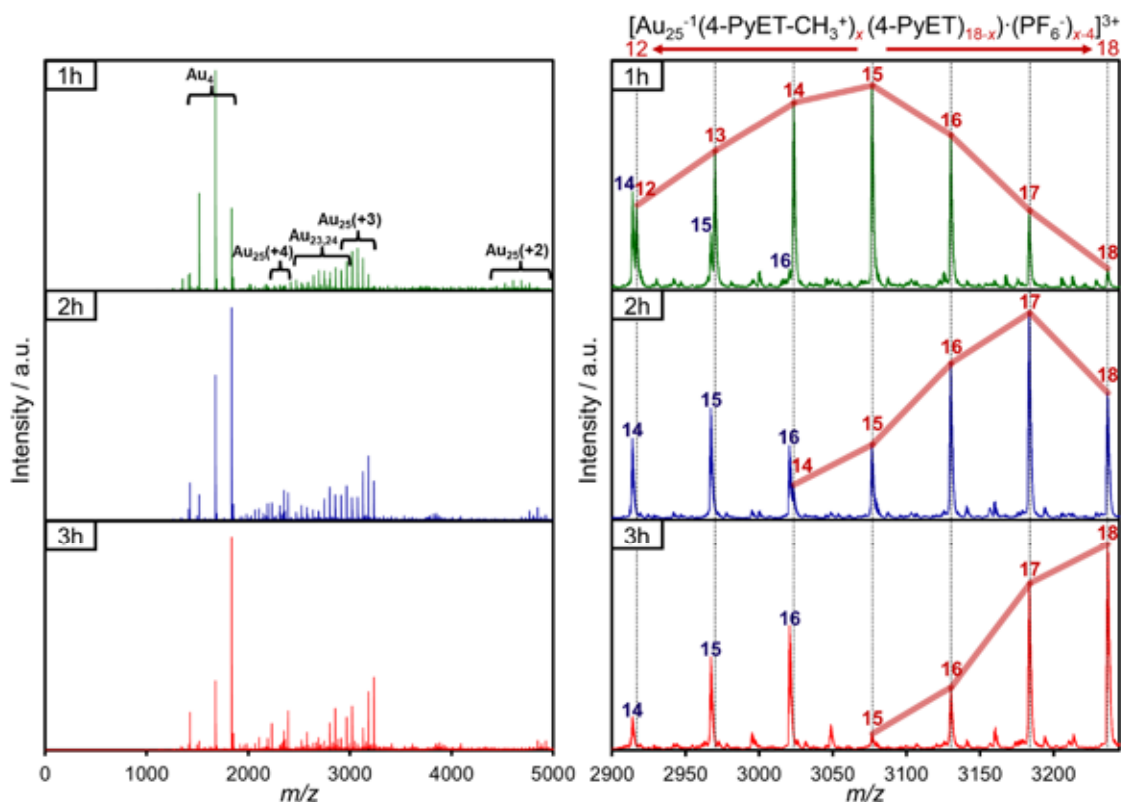


Figure 3 Positive-mode ESI-MS of the samples after different numbers of reaction cycles with TfOMe (left), and the expanded ESI-MS of group Au₂₅(+3) (right) (The red and blue numbers indicate the x values of $[\text{Au}_{25}^{-1}(4\text{-PyET}\cdot\text{CH}_3^+)_x(4\text{-PyET})_{18-x}(\text{PF}_6^-)_{x-4}]^{3+}$ and fragmentation product $[\text{Au}_{24}^0(4\text{-PyET}\cdot\text{CH}_3^+)_x(4\text{-PyET})_{16-x}(\text{PF}_6^-)_{x-3}]^{3+}$, respectively)

corresponding cluster species; the numbers for cycles 1-3 were 15.0 (83.1%), 16.7 (92.7%), and 17.3 (95.9%), respectively. The ¹H NMR spectrum of the sample after the 3rd reaction cycle also showed a similar x value of 17.3 (96.0%), confirming that the x values calculated from the mass spectral signal intensities are reliable in the selected mass region ($m/z = 2220\text{-}4950$). The average x value gradually increased by the number of reaction cycles, and nearly per-methylated Au₂₅ clusters were successfully obtained after 3 cycles. By further increasing the number of reaction cycles to 4 (4h in total), more clusters, with $x=18$, could be produced; however they exhibited more impurity peaks due to their decomposition. The compositions and charge assignments of the observed Au₂₅ cluster peaks are summarized in Table 1.

Table 1 The compositions and charge assignments of the observed Au₂₅ cluster peaks in Figure 3

<i>x</i> value	Composition	1h <i>m/z</i> (obs.)	2h <i>m/z</i> (obs.)	3h <i>m/z</i> (obs.)	<i>m/z</i> (calc.)
Total charge +2 : Au ₂₅ ⁻¹ (4-PyET-CH ₃ ⁺) _{<i>x</i>} (4-PyET) _{18-<i>x</i>} (PF ₆ ⁻) _{<i>x</i>3}					
11	Au ₂₅ ⁻¹ (4-PyET-CH ₃ ⁺) ₁₁ (4-PyET) ₇ (PF ₆ ⁻) ₈	4368.38	-	-	4368.40
12	Au ₂₅ ⁻¹ (4-PyET-CH ₃ ⁺) ₁₂ (4-PyET) ₆ (PF ₆ ⁻) ₉	4448.39	-	-	4448.40
13	Au ₂₅ ⁻¹ (4-PyET-CH ₃ ⁺) ₁₃ (4-PyET) ₅ (PF ₆ ⁻) ₁₀	4528.38	-	-	4528.38
14	Au ₂₅ ⁻¹ (4-PyET-CH ₃ ⁺) ₁₄ (4-PyET) ₄ (PF ₆ ⁻) ₁₁	4608.36	4608.36	-	4608.38
15	Au ₂₅ ⁻¹ (4-PyET-CH ₃ ⁺) ₁₅ (4-PyET) ₃ (PF ₆ ⁻) ₁₂	4688.37	4688.38	4688.31	4688.37
16	Au ₂₅ ⁻¹ (4-PyET-CH ₃ ⁺) ₁₆ (4-PyET) ₂ (PF ₆ ⁻) ₁₃	4768.35	4768.36	4768.37	4768.36
17	Au ₂₅ ⁻¹ (4-PyET-CH ₃ ⁺) ₁₇ (4-PyET) ₁ (PF ₆ ⁻) ₁₄	4848.33	4848.36	4848.36	4848.36
18	Au ₂₅ ⁻¹ (4-PyET-CH ₃ ⁺) ₁₈ (PF ₆ ⁻) ₁₅	-	4928.34	4928.34	4928.35
Total charge +3 : Au ₂₅ ⁻¹ (4-PyET-CH ₃ ⁺) _{<i>x</i>} (4-PyET) _{18-<i>x</i>} (PF ₆ ⁻) _{<i>x</i>4}					
12	Au ₂₅ ⁻¹ (4-PyET-CH ₃ ⁺) ₁₂ (4-PyET) ₆ (PF ₆ ⁻) ₈	2917.30	-	-	2917.28
13	Au ₂₅ ⁻¹ (4-PyET-CH ₃ ⁺) ₁₃ (4-PyET) ₅ (PF ₆ ⁻) ₉	2970.62	-	-	2970.61
14	Au ₂₅ ⁻¹ (4-PyET-CH ₃ ⁺) ₁₄ (4-PyET) ₄ (PF ₆ ⁻) ₁₀	3023.94	3023.95	-	3023.94
15	Au ₂₅ ⁻¹ (4-PyET-CH ₃ ⁺) ₁₅ (4-PyET) ₃ (PF ₆ ⁻) ₁₁	3077.27	3077.28	3077.27	3077.27
16	Au ₂₅ ⁻¹ (4-PyET-CH ₃ ⁺) ₁₆ (4-PyET) ₂ (PF ₆ ⁻) ₁₂	3130.59	3130.60	3130.61	3130.60
17	Au ₂₅ ⁻¹ (4-PyET-CH ₃ ⁺) ₁₇ (4-PyET) ₁ (PF ₆ ⁻) ₁₃	3183.92	3183.92	3183.93	3183.92
18	Au ₂₅ ⁻¹ (4-PyET-CH ₃ ⁺) ₁₈ (PF ₆ ⁻) ₁₄	3237.24	3237.25	3237.25	3237.25
Total charge +4 : Au ₂₅ ⁻¹ (4-PyET-CH ₃ ⁺) _{<i>x</i>} (4-PyET) _{18-<i>x</i>} (PF ₆ ⁻) _{<i>x</i>5}					
14	Au ₂₅ ⁻¹ (4-PyET-CH ₃ ⁺) ₁₄ (4-PyET) ₄ (PF ₆ ⁻) ₉	2231.72	-	-	2231.71
15	Au ₂₅ ⁻¹ (4-PyET-CH ₃ ⁺) ₁₅ (4-PyET) ₃ (PF ₆ ⁻) ₁₀	2271.71	2271.71	2271.71	2271.71
16	Au ₂₅ ⁻¹ (4-PyET-CH ₃ ⁺) ₁₆ (4-PyET) ₂ (PF ₆ ⁻) ₁₁	2311.70	2311.71	2311.70	2311.70
17	Au ₂₅ ⁻¹ (4-PyET-CH ₃ ⁺) ₁₇ (4-PyET) ₁ (PF ₆ ⁻) ₁₂	2351.70	2351.70	2351.69	2351.70
18	Au ₂₅ ⁻¹ (4-PyET-CH ₃ ⁺) ₁₈ (PF ₆ ⁻) ₁₃	2391.69	2391.69	2391.69	2391.69

The isotope distributions matched well with the simulated isotope patterns. The well-known fragmentation product [Au₄⁰(4-PyET-CH₃⁺)_{*x*}(4-PyET)_{4-*x*}(PF₆⁻)_{*x*-1}]¹⁺ (1 ≤ *x* ≤ 4) was also observed. Moreover, the fragmentation products during the ESI process [Au₂₄⁰(4-PyET-CH₃⁺)_{*x*}(4-PyET)_{16-*x*}(PF₆⁻)_{*x*-3}]³⁺ (8 ≤ *x* ≤ 16) and [Au₂₃⁰(4-PyET-CH₃⁺)_{*x*}(4-PyET)_{15-*x*}(PF₆⁻)_{*x*-3}]³⁺ (8 ≤ *x* ≤ 15) were observed for Au₂₅(SR)₁₈; these corresponded to losses of Au₁-SR₂ and Au₂-SR₃. Interestingly, like

those of the whole Au₂₅ clusters, the *x* values of these fragmentation products also increased with the number of reaction cycles.

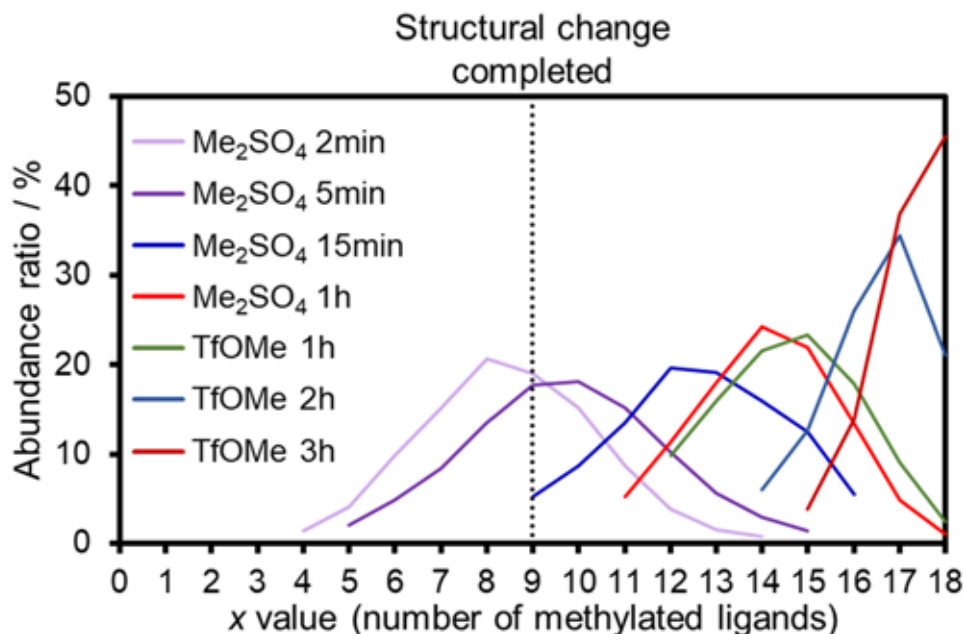


Figure 4 The abundance ratios of each cluster species with different *x* values under representative conditions

We also evaluated the weaker methylating reagent, Me₂SO₄, by varying the reaction time and number of reaction cycles; this gave clusters with various *x* values. Specifically, those with *x*=8.5, 9.7, 12.6, and 14.1 were formed by reactions with Me₂SO₄ for times of 2, 5, 15, and 60 min, respectively. The abundance ratios of each cluster species with different *x* values, determined by the intensities of their ESI-MS peaks, are shown in Figure 4. Monitoring the reaction with Me₂SO₄ revealed that the absorption spectral changes (i.e., the structural change of Au₂₅ core) were completed at 15 min, where the minimum *x* value of the contained Au clusters was 9. These observations indicate that the structural changes are complete when approximately half number of the surface Py groups are cationized. To further understand the mechanisms of the spectral and structural changes caused by the dense surface charges, we are currently isolating each cluster species and analyzing them by single-crystal X-ray structure analysis.

4. Conclusion

We have demonstrated a novel method for obtaining cationized Au clusters via the surface Menshutkin S_N2 reaction. By changing the methylating reagent, reaction time, and number of reaction cycles, we succeeded in controlling the number of methylated ligands (*x*); an *x* of approximately 18 (i.e., fully methylated Au₂₅(4-PyET-CH₃⁺)₁₈) was obtained under the optimal condition. This work proposed not only a new synthetic pathway for cationized Au clusters, but also provides a novel idea for diversifying the R-groups of molecular metal clusters through the surface chemical reaction.

Acknowledgement

Y.I. thanks financial supports from JFE 21st Century Foundation.

謝辞

本研究は公益財団法人 JFE21 世紀財団研究助成により行われました。ここに記して感謝申し上げます。

Reference

- (1) Li, G.; Jin, R. Atomically Precise Gold Nanoclusters as New Model Catalysts. *Acc. Chem. Res.* **2013**, *46*, 1749–1758.
- (2) Wan, X. K.; Wang, J. Q.; Nan, Z. A.; Wang, Q. M. Ligand effects in catalysis by atomically precise gold nanoclusters. *Sci. Adv.* **2017**, *3*, No. e1701823.
- (3) Guan, G.; Zhang, S. Y.; Cai, Y.; Liu, S.; Bharathi, M. S.; Low, M.; Yu, Y.; Xie, J.; Zheng, Y.; Zhang, Y. W., Han, M. Y. Convenient Purification of Gold Clusters by Co-Precipitation for Improved Sensing of Hydrogen Peroxide, Mercury Ions and Pesticides. *Chem. Commun.* **2014**, *50*, 5703–5705.
- (4) Shen, R., Liu, P., Zhang, Y., Yu, Z., Chen, X., Zhou, L., Nie, B; Żaczek, A.; Chen, J; Liu, J. Sensitive Detection of Single-cell Secreted H₂O₂ by Integrating a Microfluidic Droplet Sensor and Au Nanoclusters. *Anal. Chem.* **2018**, *90*, 4478–4484.
- (5) Zheng, K.; Setyawati, M. I.; Leong, D. T.; Xie, J. Surface Ligand Chemistry of Gold Nanoclusters Determines Their Antimicrobial Ability. *Chem. Mater.* **2018**, *30*, 2800–2808.
- (6) Zheng, K.; Setyawati, M. I.; Leong, D. T.; Xie, J. Antimicrobial Gold Nanoclusters. *ACS Nano*, **2017**, *11*, 6904–6910.
- (7) Chen, Y.; Zeng, C.; Kauffman, D. R.; Jin, R. Tuning the Magic Size of Atomically Precise Gold Nanoclusters via Isomeric Methylbenzenethiols. *Nano Lett.* **2015**, *15*, 3603–3609.

- (8) Yan, J.; Teo, B. K.; Zheng, N. Surface Chemistry of Atomically Precise Coinage-Metal Nanoclusters: From Structural Control to Surface Reactivity and Catalysis. *Acc. Chem. Res.* **2018**, *51*, 3084–3093.
- (9) Ackerson, C. J.; Jadzinsky, P. D.; Kornberg, R. D. Thiolate Ligands for Synthesis of Water-Soluble Gold Clusters. *J. Am. Chem. Soc.* **2005**, *127*, 6550–6551.
- (10) Knoppe, S.; Bürgi, T. Chirality in Thiolate-protected Gold Clusters. *Acc. Chem. Res.* **2014**, *47*, 1318–1326.
- (11) Yang, H.; Wang, Y.; Lei, J.; Shi, L.; Wu, X.; Makinen, V.; Lin, S.; Tang, Z.; He, J.; Hakkinen, H.; Zheng, L.; Zheng, N. Ligand-Stabilized Au₁₃Cu_x (x = 2, 4, 8) Bimetallic Nanoclusters: Ligand Engineering to Control the Exposure of Metal Sites. *J. Am. Chem. Soc.* **2013**, *135*, 9568–9571.
- (12) Yuan, X.; Goswami, N.; Chen, W.; Yao, Q.; Xie, J. Insights into the Effect of Surface Ligands on the Optical Properties of Thiolated Au₂₅ Nanoclusters. *Chem. Commun.* **2016**, *52*, 5234–5237.
- (13) Nel, A. E.; Mädler, L.; Velegol, D.; Xia, T.; Hoek, E. M.; Somasundaran, P.; Klaessig, F.; Castranova, V.; Thompson, M. Understanding biophysicochemical interactions at the nano-bio interface. *Nat. Mater.* **2009**, *8*, 543–557.
- (14) Ishida, Y.; Narita, K.; Yonezawa, T.; Whetten, R. L. Fully Cationized Gold Clusters: Synthesis of Au₂₅(SR⁺)₁₈. *J. Phys. Chem. Lett.* **2016**, *7*, 3718–3722.
- (15) Narita, K.; Ishida, Y.; Yonezawa, T.; Huang, Z. Super Polycationic Molecular Compounds: Au₁₄₄(SR⁺)₆₀ Clusters. *J. Phys. Chem. C* **2019**, *123*, 21768–21773.
- (16) Huang, Z.; Ishida, Y.; Narita, K.; Yonezawa, T. Kinetics of Cationic-Ligand-Exchange Reactions in Au₂₅ Nanoclusters. *J. Phys. Chem. C* **2018**, *122*, 18142–18150.
- (17) Fields-Zinna, C. A.; Sardar, R.; Beasley, C. A.; Murray, R. W. Electrospray Ionization Mass Spectrometry of Intrinsically Cationized Nanoparticles, [Au_{144/146}(SC₁₁H₂₂N(CH₂CH₃)₃³⁺)_X⁻(S(CH₂)₅CH₃)_Y]^{X+}. *J. Am. Chem. Soc.* **2009**, *131*, 16266–16271.
- (18) Gunawardene, P. N.; Corrigan, J. F.; Workentin, M. S. Golden Opportunity: A Clickable Azide-Functionalized [Au₂₅(SR)₁₈]⁻ Nanocluster Platform for Interfacial Surface Modifications, *J. Am. Chem. Soc.* **2019**, *141*, 11781–11785.
- (19) Cui, X.; Wang, J.; Liu, B.; Ling, S.; Long, R.; Xiong, Y. Turning Au Nanoclusters Catalytically Active for Visible-Light-Driven CO₂ Reduction through Bridging Ligands, *J. Am. Chem. Soc.* **2018**, *140*, 16514–16520.
- (20) Menshutkin, N. Beiträge zur Kenntnis der Affinitätskoeffizienten der Alkylhaloide und der organischen Amine. *Z. Phys. Chem.* **1890**, *5*, 589–600.

- (21) Huang, Z.; Ishida, Y.; Yonezawa, T. Basic $[\text{Au}_{25}(\text{SCH}_2\text{CH}_2\text{Py})_{18}]^- \cdot \text{Na}^+$ Clusters: Synthesis, Layered Crystallographic Arrangement, and Unique Surface Protonation. *Angew. Chem., Int. Ed.* **2019**, *58*, 13411–13415.
- (22) Negishi, Y.; Chaki, N. K.; Shichibu, Y.; Whetten, R. L.; Tsukuda, T. Origin of Magic Stability of Thiolated Gold Clusters: a Case Study on $\text{Au}_{25}(\text{SC}_6\text{H}_{13})_{18}$. *J. Am. Chem. Soc.* **2007**, *129*, 11322–11323.
- (23) Zhu, M.; Aikens, C. M.; Hollander, F. J.; Schatz, G. C.; Jin, R. Correlating the Crystal Structure of a Thiol-Protected Au_{25} Cluster and Optical Properties. *J. Am. Chem. Soc.* **2008**, *130*, 5883–5885.
- (24) Zhu, M.; Chan, G.; Qianb, H.; Jin, R. Unexpected Reactivity of $\text{Au}_{25}(\text{SCH}_2\text{CH}_2\text{Ph})_{18}$ Nanoclusters with Salts, *Nanoscale*, **2011**, *3*, 1703–1707.